Mimicking Natural Laminar to Turbulent Flow Transition – A Systematic CFD Study Using PAB3D

S. Paul Pao* and Khaled S. Abdol-Hamid*
NASA Langley Research Center, Hampton, Virginia 23681

For applied aerodynamic computations using a general purpose Navier-Stokes code, the common practice of treating laminar to turbulent flow transition over a non-slip surface is somewhat arbitrary by either treating the entire flow as turbulent or forcing the flow to undergo transition at given trip locations in the computational domain. In this study, the possibility of using the PAB3D code, standard k-ε turbulence model, and the Girimaji explicit algebraic stresses model to mimic natural laminar to turbulent flow transition was explored. The sensitivity of flow transition with respect to two limiters in the standard k-ε turbulence model was examined using a flat plate and a 6:1 aspect ratio prolate spheroid for our computations. For the flat plate, a systematic dependence of transition Reynolds number on background turbulence intensity was found. For the prolate spheroid, the transition patterns in the three-dimensional boundary layer at different flow conditions were sensitive to the free stream turbulence viscosity limit, the reference Reynolds number and the angle of attack, but not to background turbulence intensity below a certain threshold value. The computed results showed encouraging agreements with the experimental measurements at the corresponding geometry and flow conditions.

Nomenclature

C_f	=	skin friction coefficient
c_∞	=	free stream speed of sound, *m/s*
I_t	=	background turbulence intensity, fraction of freestream velocity
M_t	=	turbulence Mach number
$M_{t\text{-}max}$	=	maximum turbulence Mach number near a solid surface
M_∞	=	free stream Mach number
L	=	reference length, *m*
Re_L	=	unit Reynolds number based on reference length
Re_x	=	Reynolds number based on streamwise distance from the flat plate leading edge
u'	=	turbulence velocity, *m/s*
u^+	=	law of the wall velocity
x	=	streamwise distance from the flatplate leading edge, *m*
y^+	=	law of the wall distance from the wall
$\Delta_{dissipation-free}$	=	length-scale of dissipation for turbulent kinetic energy in the free stream
μ_t	=	laminar viscosity coefficient, *Pascal·s*
μ_t	=	turbulent viscosity coefficient, *Pascal·s*

I. Introduction

For a wide class of applied aerodynamics computations using a general purpose Navier-Stokes code, the common practice of treating laminar to turbulent flow transition over a non-slip surface is somewhat arbitrary. When a turbulence model is chosen for a given computation, the code would either treat the entire flow as turbulent by

* Research Engineer, Configuration Aerodynamics Branch, MS-499, AIAA Associate Fellow.

default, or provide for the user a method to specify trip locations in the computational grid such that the flow will be forced to undergo transition at or a short distance downstream of the user specified trip location. It can be challenging to specify a physically realistic transition location.

However, in many of the CFD applications using PAB3D[1-3] with the trip method, the computed flows usually follows the laminar/turbulent flow types as intended by the trip placement. Carlson[4] described in detail the boundary layer properties and the accurate predictions of skin friction coefficient upstream and downstream of the trip point as compared to the classical Blasius theory, the 1/5th power law, and the White exact theory. In other cases, however, the flow may first respond to the trip, become turbulent, and then re-laminarize shortly after because of a favorable pressure gradient. In still other examples, the flow solution had already made the transition before the trip location and mimicked a natural transition. In the last example, however, it was not known whether such mimicking behavior was incidental or as a result of better than expect representation of flow physics represented by the k-ε turbulence closure and the algebraic Reynolds stresses mode in the Navier-Stokes code.

In order to gain some understanding for this issue, the authors initially performed a systematic set of calculations of flows over a flat plate without numerical tripping to explore the sensitivity of the transition Reynolds number as a function of certain key turbulence model parameters in the PAB3D code. The computed results are then examined in light of classical experimental evidences in the literature.

A typical two-equation turbulence closure model requires limiters. Relevant to this study are the limiter for minimum turbulence intensity in terms of a turbulent Mach number, $M_t|_{limit}$, and a limiter for the free stream turbulence viscosity as a fraction of the laminar viscosity, $\mu_t/\mu_\ell|_{limit}$. We can explicitly relate $M_t|_{limit}$ to the background turbulence intensity, I_t, in the flow. Similarly, one can relate $\mu_t/\mu_\ell\,|_{limit}$ to the length scale of turbulent kinetic energy dissipation in the free-stream. The user can specify different values through a user-input file at run time. From the literature on transition measurements, it is recognized that the transition Reynolds number is sensitive to both of these parameters. Hence, developing a rational approach to explore the computational consequences when these two parameters are varied for flow simulations over two- and three-dimensional configurations was the focus of the current work. For this initial study, a flat plate was chosen to study two-dimensional flow transition, and a 6:1 aspect ratio prolate spheroid for three-dimensional flow transition. While the flat plate is perhaps the simplest of all viscous flow configurations, any three-dimensional configuration comes with its own specific flow characteristics not shared by other three dimensional configurations. Hence, a 6:1 aspect ratio prolate spheroid was chosen not because its simple shape but because the computed results can readily be compared to the experimental measurements of flow transition for this shape reported by Kreplin et al.[5-8].

II. The Flat Plate Study

A. The Structured Mesh and the Computational Domain

A fine grid was constructed over a 10-meter long flat plate. The computational domain height above the plate is 2 meters, and it includes also a 0.5-meter long inflow domain upstream of the flat plate leading edge. The first grid size in the streamwise direction at the flat plate leading edge is 0.025 mm. The grid size expansion ratio started from approximately 1.10 near the leading edge and slowed to 1.005 at 2 meters downstream. The largest cell at the out flow boundary is 60 mm. In the direction normal to the flat plate, the grid expansion ratio is approximately 1.08 throughout the boundary layer. During the computation, it was verified that the first grid height at fine grid level corresponds to a y^+ value of 0.074. There are approximately 70 grid cells below a normalized boundary layer height of $y^+ = 1000$. The computations were carried out using grid sequencing through coarse, medium, and fine grid levels. A large flat plate computational domain in length and height was chosen for two reasons. The first was to avoid the influence of the outflow boundary condition on the development of the boundary layer over the flat plate. The second was to allow ample length for the numerical solution to develop freely and to decide, without user intervention, whether a flow transition would occur for each computation.

B. Computational Procedure and Discussion of Results

It is known in wind tunnel testing that the natural transition Reynolds number, Re_x, is influenced by the wind tunnel background turbulence intensity, I_t. It is also known in the literature, for example Rodi[9], that the transition Reynolds number Re_x may depend on the spatial scale of turbulent kinetic energy dissipation in the free stream, $\Delta_{dissipation-free}$. These quantities are related to the turbulent Mach number limit, $M_t|_{limit}$, and the turbulent viscosity limit, $\mu_t/\mu_\ell|_{limit}$ by:

$$I_t = u'_{Background} \Big/ M_\infty c_\infty = \sqrt{2/3}\, M_t\,|_{Limit} \Big/ M_\infty$$

And

$$\Delta_{dissipation-free} = 9.07 \frac{\mu_t / \mu_\ell\,|_{Limit}}{I_t} / \mathrm{Re}_L$$

In the second equation, Re_L is a Reynolds number based on a reference length. It can simply be a unit Reynolds number if L is chosen as a unit length such as one foot or one meter.

The dependence of the transition turbulence on the background turbulence intensity, I_t, over a range of values from I_t = 0.0383 to I_t = 1.149 percent was examined first. The results are shown in Figure 1 where the skin friction coefficient is given as a function of the Reynolds number based on the distance from the flat plate leading edge, Re_x. Each curve in Fig. 1 is computed for a different I_t value. The flow over the flat plate is initially laminar, as shown by the skin friction coefficient follows the Blasius curve. When the computed boundary layer over the flat plate makes the transition from a laminar to a turbulent flow, the skin friction coefficient jumps to a value that initially overshoots and then settles down to values consistent with the 1/5th power law or the White exact theory curves for turbulent boundary layers over a flat plate. Similar to the practice of other investigators, the transition Reynolds number was defined as the point where each curve attained the lowest skin friction coefficient near the Blasius reference value.

The authors were surprised to find that the transition Re_x location actually varied systematically with the input background turbulence intensity via $M_t|_{limit}$ in the PAB3D code. Note however, the computed flow over the flat plate at the two lowest values of background turbulence intensity, I_t = 0.0383 and I_t = 0.0767 percent, the skin friction coefficient deviated from the Blasius theoretical curve at values greater than Re_x = 2.0E+6. Furthermore, the I_t = 0.0383 case did not make the transition to turbulent flow at the end of the 10-meter flat plate at which point the Re_x equals 16.09E+6. Two factors may have been responsible for the skin friction coefficient deviation relative to the Blasius curve. First, the distance from the flat plate leading edge at Re_x = 2.0E+6 is approximately 1.26 meters. At that location, the streamwise cell size of the computational mesh is nominally 16 mm. At the leading edge of the flat plate, a cell size of 0.025mm was used to minimize the magnitude of the numerically created impulse of turbulent kinetic energy due to the large gradients created by the velocity discontinuity when the free stream velocity suddenly decelerates to zero on the no-slip surface at the flat plate leading edge. The grid cell size downstream from the leading edge then expanded at a slow rate to ensure proper turbulence development over the flat plate. When the cell grew to sizes near 16 mm, it could have been too large for the proper development of the boundary layer velocity profile and the eventual transition from laminar to turbulence flow. Second, it could simply be a problem of round off errors in a single precision computation we have used during this part of the investigation.

Next a set of computations was performed to examine the dependence of transition Re_x on the parameter $\mu_t/\mu_\ell\,|_{limit}$. The results are shown in Figure 2. The study shows the impact of $\mu_t/\mu_\ell\,|_{limit}$ on transition Re_x is small even when varied over a range from 0.3 to 5.0, (a factor of 16). As another check on the quality of the flat plate boundary layer simulation, the u^+ versus y^+ plots at two typical streamwise locations on the flat plate in the turbulent boundary layer region is shown in Figure 3. The profiles show self-similarity in the viscous sublayer, the buffer zone, and the log layer. The profiles differ only in the wake region, which is expected according to classical theoretical analysis.

To establish a trend for this computational investigation, the transitional Re_x as a function of freestream background turbulence intensity, I_t, is plotted on double logarithmic scales with Re_x place on the horizontal axis. The result is shown in Figure 4. First, a straight line can be faired through the computed points (square symbols). It provides an indication of the trend as a power law. Two sets of experimental data points are also shown in this figure. The first

set has only two points represented by the upright triangle symbols for empirically established wind tunnel practice. The commonly assumed typical tunnel transition Re_x is 3.0E+05. For each given tunnel turbulence intensity, a factor is assigned to estimate the transition Re_x. For example, a transition factor of 2.0 is assigned to tunnel turbulence intensity of 1%, a higher than normal tunnel background turbulence intensity. That would indicate transition might occur at Re_x as low as 1.5E+05. The second set of data, shown in the figure as six inverted-triangle symbols, represents the data used by Warren and Hassan[10] which came originally from Schubauer et al.[11-12]. The three data points for the higher tunnel turbulence intensities show a high transition Re_x than the computed values. However, the relation between turbulence intensity and Re_x is similar to the computed trend. The three data points at lower tunnel turbulence intensities show a constant transition Re_x. In the report by Schubauer and Skramstad[11], the authors noted that after a certain level of reduction of turbulence intensity in the tunnel, flow transition could be triggered by disturbances such as high acoustic intensity in the tunnel, and not by the Tollmein-Schlichting wave instability in the boundary layer. Hence, the transition Reynolds number no longer depends on the background tunnel turbulence intensity levels below a certain threshold value. In summary, the computed transition Reynolds number versus the background turbulence intensity trend is similar to that shown by the experimental data collectively from two different sources. If we compare the computed Re_x to those measured by Schubauer and Skramstad, the computed values are approximately a factor of 2.0 smaller for a given I_t. That is, transition is predicted prematurely by the computation.

Another factor, which was probably not anticipated in the earlier experiments for flat plate transition, is the turbulence intensity measured near the flow-straightening screen could decay downstream as indicated by Craft, Launder, and Suga[13], and Chen, Lien, and Leschziner[14]. If the background turbulence decay in the tunnel is factored into the computation, one would expect that the transition Re_x would have higher values for a given I_t. This was done in a set of exploratory computations in this study by assuming the turbulence intensity will decay by 50% from the beginning to the end of the computational domain. Fig. 5 shows the results for three initial values of I_t and the transition Re_x by assuming no decay and decay by 50% at the end of the computational domain. The computed transition Reynolds numbers, Re_x, with 50% background turbulence intensity decay now appear much closer to the Schubauer data. The authors would like to point out that this exercise was not intending to match the data by assuming a turbulence intensity decay, rather it is used as an example to show that differences between computed and experimental data could come from a number of sources. Hence, one must consider carefully all the relevant computational and experimental details for future studies of flat plate flow transition simulation and the subsequent comparison between computed and measured data.

III. The 6:1 Prolate Spheroid Study

A. The Structured Mesh and the Computational Domain

The 6:1 prolate spheroid measurements by Kreplin et al.[5-8] used a model 2.4 meter in length in the DFVLR (now DLR) 3m x 3m wind tunnel. As was with the flat plate, a very fine grid was constructed for the prolate spheroid. In some sense, it is finer than the flat plate grid in the first part of this paper. There is a key difference between the flat plate grid and the grid for the prolate spheroid. For the flat plate, a very small grid spacing, 0.025mm, was selected to handle the velocity discontinuity at the leading edge of the plate. In a three-dimensional configuration, the flow attachment to the body occurs at a stagnation line, and flow velocities remain continuous. Hence, the main emphasis in this case is to select surface grid sizes for the proper development of the laminar and turbulent boundary layers on the body of the spheroid. The grid was divided into two zones: an interior domain surrounding the spheroid and an exterior domain representing the inviscid far-field away from the spheroid as show in Fig. 6. The near field had a total of 608 grid cells in the longitudinal direction, 192 grid cells around half of the circumference, and 40 grid cells from the prolate spheroid surface to the beginning of far-field domain. The exterior domain had a total of 304 cells in the longitudinal direction, 96 cells around the half-circumference, and 40 grid cells as a continuation of the grid cells in a direction normal to the spheroid surface. The far field boundary was approximately 24 meters away from the center of the spheroid in all directions. The first grid height is 0.336E-02 mm that corresponds to y^+ values of less than 0.4 for the higher Reynolds number cases in this study. On the prolate spheroid surface, the grid had an almost uniform spacing, with a higher cell density at the two ends of the spheroid. The maximum axial spacing near the equator of the spheroid was 4.2 mm. The circumferential spacing was just less than one degree per cell. The physical grid spacing around the circumference at the equator was 3.25 mm. The polar singularity at the two ends of the spheroid was removed by replacing the two conical sectors by Cartesian grids, which were point continuous with the original spherical grid. In summary, the overall grid had a spherical topology, and the grid covers half of the

spheroid with a symmetry plane along a meridian of the spheroid. The total grid cell count was 5.84 million. For efficient parallel computing purposes, the original monolithic grid was divided into 52 blocks. Most of the computations used 26 nodes per case on Linux clusters.

B. Computational Procedure using PAB3D

Kreplin et al.[8] mentioned four cases of shear stress and limited transition measurements for the 6:1 prolate spheroid model inclined with respect to the tunnel flow of 10° and 30°, and two tunnel speeds at 10 m/s and 45 m/s. All four cases were computed using the Girimaji explicit algebraic stresses model together with the standard k-ε turbulence model. One difference from the flat plate cases is that we used the constant time stepping for reasons that will become clear later in the discussion of results. In order to gain accuracy in terms of surface smoothness and numerical round off error, double precision was used for both the grid and the computations. Each solution started with nominally 1000 to 2000 time steps at medium grid level, and then continued at fine grid level for as many time steps as necessary to obtain a well-converged solution. While it is not the only criterion used, the RMS-residue of the solutions normally dropped between four to five orders of magnitude from beginning to end of these computations. The tunnel velocities in the DFVLR 3m x 3m wind tunnel were 10 m/s and 45 m/s and correspond to M = 0.029 and M = 0.132, respectively. The corresponding Re_L were 1.6 E+6 and 7.2 E+6, based on the 2.4 meter length of the spheroid. For numerical accuracy reasons in the low subsonic speed range, a Mach number of M = 0.264 (twice of M = 0.132) was used to compute all the cases. The free stream static pressure in the computation was adjusted to match the computed Re_L to each of the wind tunnel measurements.

For this part of the flow transition mimicking study, the $M_t|_{limit}$ and the $\mu_t/\mu_\ell\,|_{limit}$ parameters were again varied in the PAB3D code. However, the overall flow physics considerations for natural flow transition are much more complex. Relevant factors would include surface pressure gradient, surface roughness and discontinuities, cross flow velocity and vorticity in the boundary layer, compressibility effect, and potentially many others. The Reynolds number and angles-of-attack dependences are considered in the computations, but with merely two values for each parameter. Hence, this three-dimensional flow transition study is very limited in scope and exploratory in nature. Any conclusion one may draw from this study would be tentative and should be viewed with caution.

C. Prolate Spheroid Computations and Comparisons to Measured Data

The authors were surprised when test computation showed that the simulated transition patterns had very little sensitivity to $M_t|_{limit}$. The only observed solution behavior for varying $M_t|_{limit}$ was that the flow over the surface of the spheroid quickly becomes turbulent if the $M_t|_{limit}$ value was too high. When the value of $M_t|_{limit}$ was reduced to below that threshold, the transition pattern remained the same for a given value of $\mu_t/\mu_\ell\,|_{limit}$. The transition pattern is, however, sensitive to the $\mu_t/\mu_\ell\,|_{limit}$. This is opposite to the results found earlier for the flat plate computations. For the solutions presented in this paper, $M_t|_{limit}$ was simply fixed at a low value of $M_t|_{limit}$ = 0.0004. It corresponds to a background turbulence intensity of I_t = 0.13% and is within the range of what one would expect in a high quality subsonic research wind tunnel.

After it had been determined the transition pattern was sensitive to $\mu_t/\mu_\ell\,|_{limit}$, the goal was to find an empirical match of the Re_L = 7.2E+6 case at 30° incline. Solutions were computed at four values of $\mu_t/\mu_\ell\,|_{limit}$: 0.1, 0.2, 0.3, and 0.4. Fig. 6 shows a summary of these four computations. A clear way to distinguish laminar boundary layer, turbulent boundary layer, and flow separation is to examine the maximum turbulence Mach number magnitude, $M_{t\text{-}max}$, and the height above the solid surface where the maximum occurs. The $M_{t\text{-}max}$ distributions over the spheroid for these four cases are shown in Fig. 7. The flow is laminar when $M_{t\text{-}max}$ is less than one percent of the free stream Mach number (M_∞ = 0.264 for these case), shown as dark blue in Fig. 7. However, if $M_{t\text{-}max}$ is near 8 to 15 percent of M_∞, shown as light blue or yellow-green, the boundary layer has made its transition to a turbulent flow state. When $M_{t\text{-}max}/M_\infty$ exceeds 20 percent, shown as yellow through red, it would normally indicate flow separation. Flow separation can easily be confirmed by other parameters such as the height of occurrence of $M_{t\text{-}max}$ or the streamline traces on the surface and within the flow volume near the spheroid. Published figures in Kreplin et al.[8] provided evidences of transition location in two ways. First, there was direct measurement of transition and flow separation locations around the circumference of the prolate spheroid at a single axial station of x/L = 0.48. According to that measurement, transition occurred at a point 70° from the bottom of the spheroid. The best match relative to the published transition location would be the solution for $\mu_t/\mu_\ell\,|_{limit}$ =0.30. A second way of inferring flow transition is

from the abrupt jumps in shear stress magnitude at all the twelve stations where measurements were reported. If that indirect indication of transition were used for comparison, then the solution computed with $\mu_t/\mu_\ell\,|_{limit}$ =0.20 could also be an acceptable match. In any case, the $\mu_t/\mu_\ell\,|_{limit}$ =0.30 was used as a match, and computations proceeded on remaining three other flow conditions with $\mu_t/\mu_\ell\,|_{limit}$ fixed at this value.

As the progress of the flow solutions during the constant time stepping process were tracked, it was observed that flow transition first occurred near the nose of the spheroid, perhaps as a consequence of the adverse pressure gradient downstream of the highlight of the configuration at a given angle of incline. As the solution advanced in time, the turbulent flow zone spread slowly downstream over the leeward side of the spheroid. At the same time, the flow separation zone was also forming, independent of the flow transition process. The time history of flow development appeared to indicate that the flow transition on the spheroid farther downstream from the nose region was induced by cross flow influences migrating progressively from one streamline to the next along the body surface, and not appeared to be governed by the growth of turbulence kinetic energy along a streamline such as was the case for the flat plate. A constant time stepping algorithm was chosen for these calculations in anticipation of the rapidly change flow in the separation zone. In hind-sight, however, the constant time stepping approach for developing a solution may have provided additional insight into the laminar to turbulent flow transition mechanism for this truly three dimensional configuration with significant surface curvature in two directions.

Two flow parameters will be examined next to provide a broader view of the solution characteristics and their comparisons to the available experimental data: the maximum values of the turbulence Mach number, $M_{t\text{-}max}$ and surface streamline traces. In Figs. 8-11, the numerical and color range for the contours remains the same as shown in Fig. 7. Figure 8 shows a set of the distribution of these parameters on the surface of the spheroid for the case of Re_L = 7.2E+6 at 30° incline. The experimentally measured transition zone, as implied by the abrupt jump in shear stress magnitude, is sketched into the figure as a band defined by two curves. The computed transition occurs earlier towards the nose than the measured shear stress jump. However, the downstream pattern agreement is quite good. The bottom parts of Fig. 8 show a comparison between the measured and the computed surface streamline traces. The computed streamline pattern on the upper body of the spheroid shows a weaker separation pattern than the measurement. The measured separation starts near x/L = 0.20, while the computed separation pattern does not start until near x/L=0.60 at best. Figure 9 shows the comparison for the case of Re_L = 7.2E+6 at 10° incline. Again, the computed transition occurred earlier towards the front of the spheroid by comparing the transition as indicated by the computed $M_{t\text{-}max}$ contours and the approximate location of the measured transition as indicated by the straight dash line across the spheroid in Fig. 8. The encouraging message, however, is that the computation automatically adjusted to a completely different transition pattern with fixed turbulence model parameters.

Figures 10 and 11 show the results for the lower Reynolds number cases, Re_L = 1.6E+6. In Fig. 10 for the 30° incline, the computed boundary layer remained laminar over the entire spheroid according to the $M_{t\text{-}max}$ magnitude and the smoothness of the streamline pattern over the spheroid. The higher $M_{t\text{-}max}$ values in the contour plot were determined to be a result of flow separation. In Fig. 11, the boundary layer over the upstream half the spheroid remained laminar, while the downstream half of the body was covered by a combination of flow separation and turbulent boundary layer. The indication of transition from a laminar to a turbulent boundary layer can be inferred through a combination of $M_{t\text{-}max}$ distribution and the streamline pattern shown in Fig. 11. The magnitude of $M_{t\text{-}max}$ indicated that the boundary layer over the leading half of the spheroid was laminar. The flow separation line in the streamline plot went smoothly in one direction. Near mid-body, however, a kink appeared along the separation line and the flow separation boundary shifted towards the leeward side of the body. This was a typical flow behavior indicating flow transition because flow separation was delayed on account of the boundary layer had become turbulent. The report by Kreplin et al. stated that the boundary layer over the entire body was laminar. This was also illustrated by measured separation line which remained straight along the entire body length. It is interesting to note that the measured flow separation line pattern showed a kink near the end of the spheroid. Such a kink did not appear in the other three measured streamline patterns by Kreplin et al.[8]. However, the original authors did not comment on this particular feature in their measurement. The significance of such a kink in the data remains unknown. Again, the encouraging message is that without changing the turbulence model limiters in the PAB3D code, the computations predicted laminar flow over most or all parts of the surface with a reduction of the Reynolds number in accordance with the experimental measurements. Finally, it was observed that, consistent with the flat plate, transition was predicted early when compared to experimental data.

IV. Summary and Concluding Remarks

A preliminary study of natural flow transition mimicking using simple two- and three-dimensional configurations have led us to believe that a Navier-Stokes code such as the PAB3D code with a standard k-ε turbulence model and a theoretically based explicit algebraic stresses model (by Girimaji) have the sensitivity to mimic laminar to turbulent flow transition in the boundary layer. For the two-dimensional flat plate case, the results have quantitatively demonstrated that the computed flow transition Reynolds number has a consistent parametric relationship to the inflow background turbulence intensity. A linear curve was fitted through the computed points on a double logarithmic plot to represent the trend of variation as a power law between the background turbulence intensity and the transition Reynolds number based on the transition point distance from the flat plate leading edge. The trend is qualitatively consistent with the empirical rules established for wind tunnel measurements and the classical flat plate laminar to turbulent flow transition data obtained by Schubauer and Skramstad. In the three-dimensional prolate spheroid computations, a complex set of flow physics issues, such as pressure gradient, cross flow streamline curvatures, compressibility effects, vorticity, and shear flow stresses came into the picture. The quantitative relationship between any of these effects and transition are recognized to be important, but has not yet been well established in the literature. Nevertheless, the 6:1 prolate spheroid flow simulation was completed for two Reynolds numbers at two angles of attack for comparison to existing data. The computed flow was found to mimic transition without specific input such as tripping, and comparisons with data showed interesting similarities in terms of flow transition characteristics. Although these computational investigations are preliminary and the comparison to data is qualitative in nature, the positive indications are very encouraging for further studies of natural flow transition mimicking using a standard Navier-Stokes solver, turbulence model, and an appropriate turbulent stresses model, preferably with a traceable theoretical basis. The authors certainly would hope that this limited study would generate interest in further theoretical and numerical research for this important subject in applied aerodynamics.

References

[1]Abdol-Hamid, Khaled S., Massey, Steven J., and Elmiligui, Alaa, "PAB3D Code Manual", Cooperative development by the Configuration Aerodynamics Branch, NASA Langley Research Center and Analytical Services & Materials, Inc. Hampton, VA.

[2]Uenishi, K. and Abdol-Hamid, K.: A Three-Dimensional Upwinding Navier-Stokes Code with k-ε Model for Supersonic Flows", AIAA 22nd Fluid and Plasmadynamic Conference, AIAA 91-1669, June 1991.

[3]Abdol-Hamid, K. S.: Implementation of Algebraic Stress Models in a General 3-D Navier-Stokes Method (PAB3D). NASA CR-4702, December 1995.

[4]Carlson, J. R.: "Applications of algebraic Reynolds stress turbulence models – Part I.: Incompressible flat plate", J. Propulsion and Power, 13 -5, 610-619, October 1997.

[5]Wilcox, David C.: Turbulence Modeling for CFD, pp.193-201, Second Ed., DCW Industries, 1998.

[6]KrepIin, H.-P., Vollmers, H., and Meier, H. U.: "Wall shear stress measurements on an inclined prolate spheroid in the DFVLR 3m x 3m Low Speed Wind Tunnel," Data Report, DFVLR IB 222-84/A 33, Gottingen, Germany., 1985.

[7]Vollmers, H., Kreplin, H.-P., Meier, H. U., and Kiihn, A.: "Measured mean velocity field around a 1:6 prolate spheroid at various cross sections," Data Report, DFVLR IB 221-85 A 08, Gottingen, Germany, 1985.

[8]Kreplin, H.-P., Vollmers, H., Meier, H. U.: "Experimental determination of wall shear stress vectors on an inclined prolate spheroid", DFVLR-AVA, Gottingen, AFFDL-TR-80-3038, 1980.

[9]Rodi, W.: "Experience with two-layer models combining the k-epsilon model with a one-equation model near the wall", AIAA Paper 91-0216, January 1991.

[10]Warren, E. S., and Hassan, H. A.: "Transition closure model for predicting transition onset", J. Aircraft, 35–5, September 1998.

[11]Schubauer, G. B., Skramstad, H. K.: "Laminar boundary layer oscillations and transition on a flat plate", NACA TR-909, April 1943.

[12]Schubauer, G. B., Klebanoff, P. S.: "Contributions to the mechanics of boundary layer transition", NACA-TR-1289, February 1955.

[13]Craft, T. J., Launder, B. E., and Suga, K.: "Prediction of turbulent transitional phenomena with a nonlinear eddy-viscosity model", J. Heat and Fluid Flow, 18, pp. 15-28, 1997.

[14]Chen, W. L., Lien, F. S., and Leschziner, M. A.: "Non-linear eddy-viscosity modeling of transitional boundary layers pertinent to turbomachine aerodynamics", J. Heat and Fluid Flow, 19, 297-306, 1998.

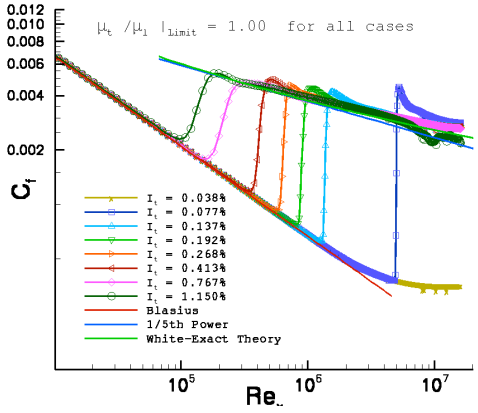

Figure 1. Skin friction coefficient as a function of Re_x over a range M_t $|_{limit}$ values showing the effect of background turbulence intensity on transition.

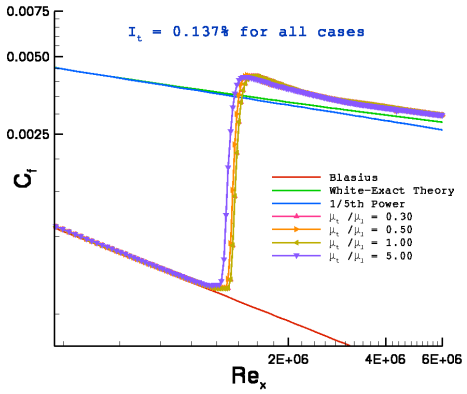

Figure 2. Skin friction coefficient as a function of Re_x over a range μ_t/μ_ℓ $|_{limit}$ values showing the effect of turbulent spatial scale on transition.

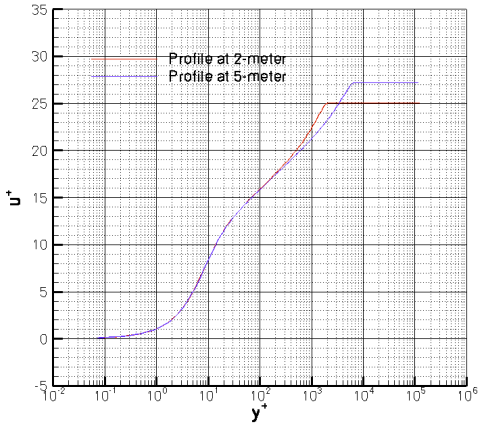

Figure 3. Normalized turbulent boundary layer profile at two different locations along the flat plate at 2 and 5 meters at one typical flow condition.

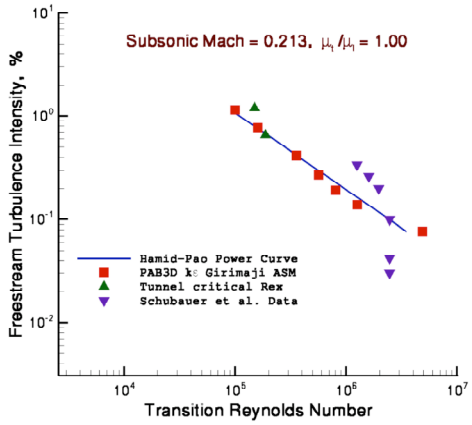

Figure 4. Power law dependence between freestream turbulence intensity and transition Reynolds number based on distance from the flat plate leading edge.

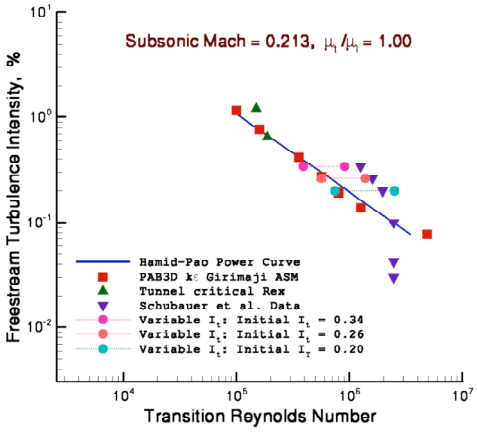

Figure 5. An exploratory study of the influence of decaying freestream turbulence intensity on transition Reynolds number.

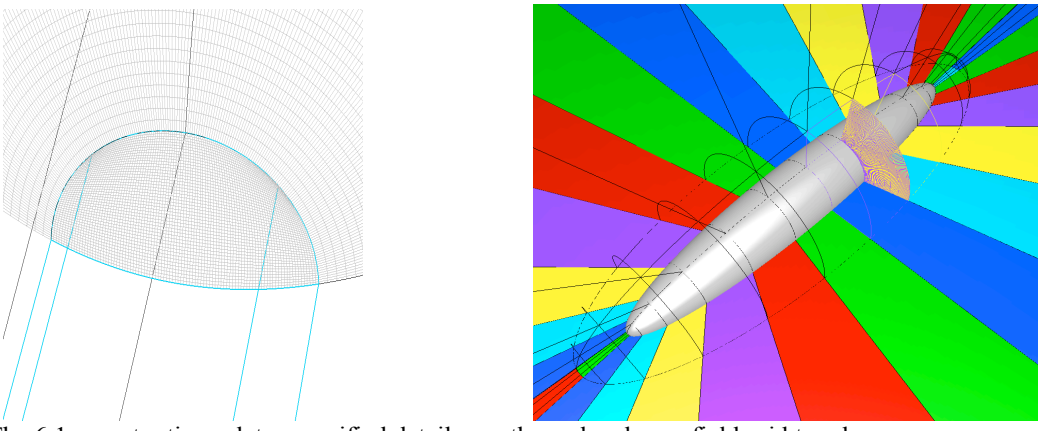

Figure 6. The 6:1 aspect ratio prolate magnified detail near the end and near-field grid topology.

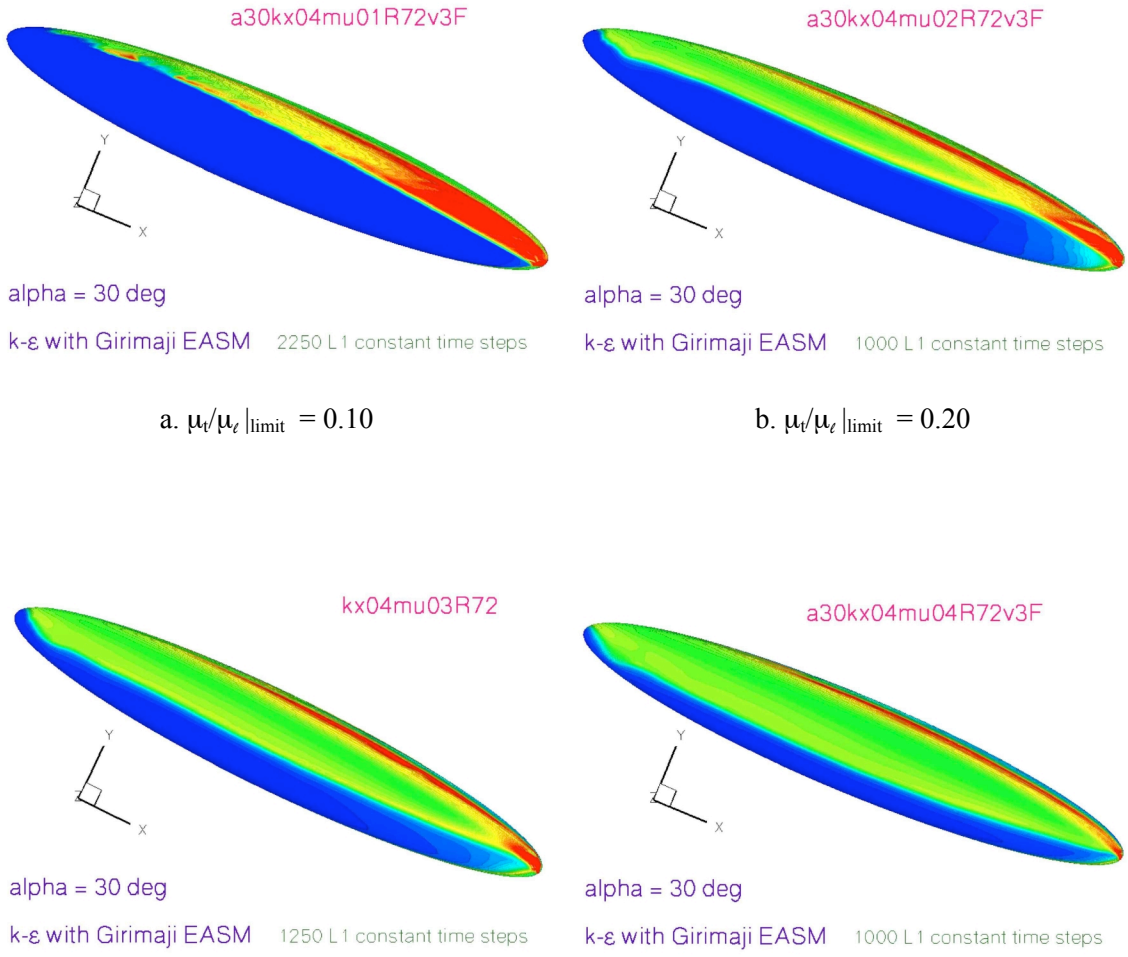

a. $\mu_t/\mu_\ell\,|_{\text{limit}} = 0.10$

b. $\mu_t/\mu_\ell\,|_{\text{limit}} = 0.20$

c. $\mu_t/\mu_\ell\,|_{\text{limit}} = 0.30$

d. $\mu_t/\mu_\ell\,|_{\text{limit}} = 0.40$

Figure 7. The effect of $\mu_t/\mu_\ell\,|_{\text{limit}}$ on the computed laminar to turbulent flow transition, as indicated by the maximum turbulence Mach number distribution over the body surface, at Re_L = 7.2E+6 and angle of attack at 30°.

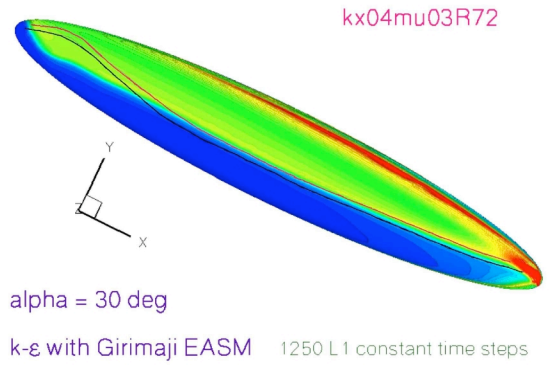

a. Distribution of $M_{t\text{-}max}$ plotted over the prolate spheroid surface

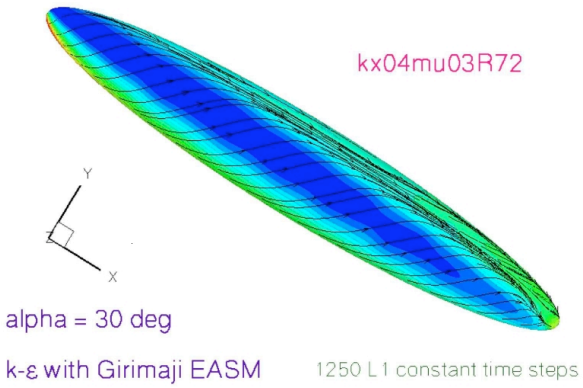

b. Computed surface streamline pattern

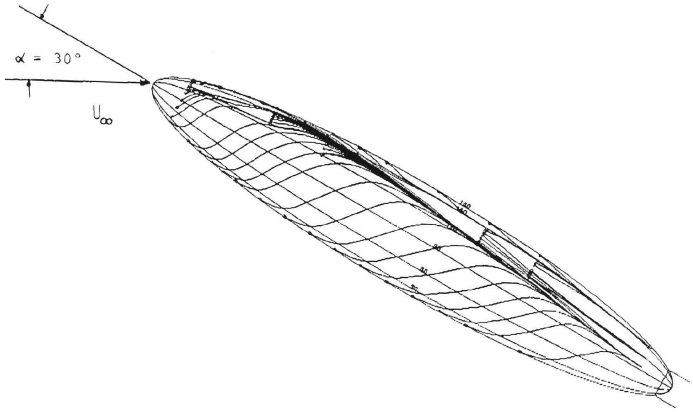

c. Surface streamlines integrated from measured velocity vector over the prolate spheroid (Kreplin, 1981).

Figure 8. Flow parameter contours and qualitative comparison to experiment solution at Re_L = 7.2E+6 and angle of attack at 30°, and $\mu_t/\mu_\ell\,|_{limit}$ = 0.30.

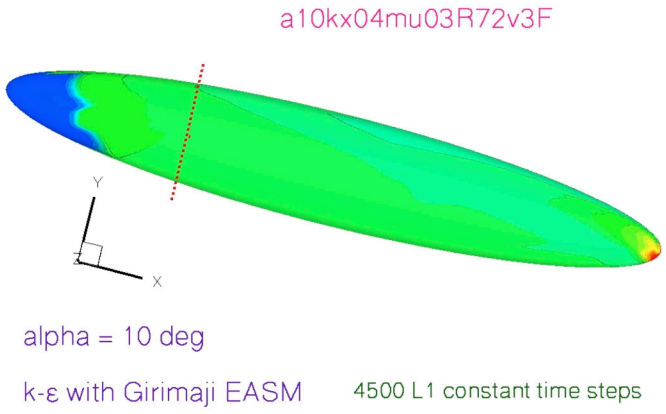

a. Distribution of $M_{t\text{-}max}$ plotted over the prolate spheroid surface

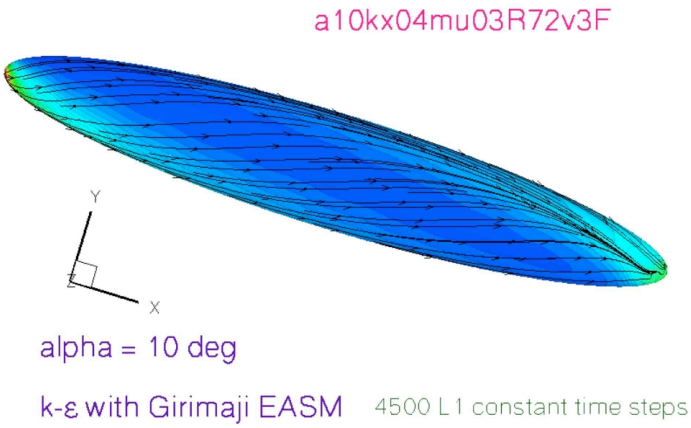

b. Computed surface streamline pattern

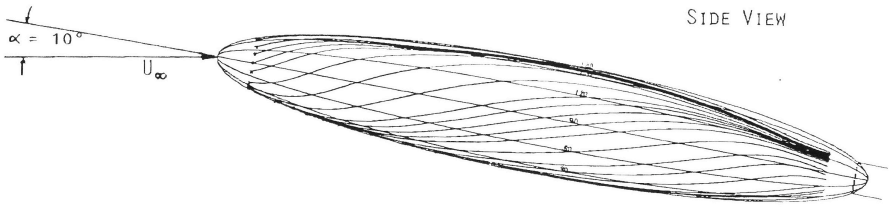

c. Surface streamlines integrated from measured velocity vector over the prolate spheroid (Kreplin, 1981).

Figure 9. Flow parameter contours and qualitative comparison to experiment solution at Re_L = 7.2E+6 and angle of attack at 10°, and $\mu_t/\mu_\ell\,|_{limit}$ = 0.30.

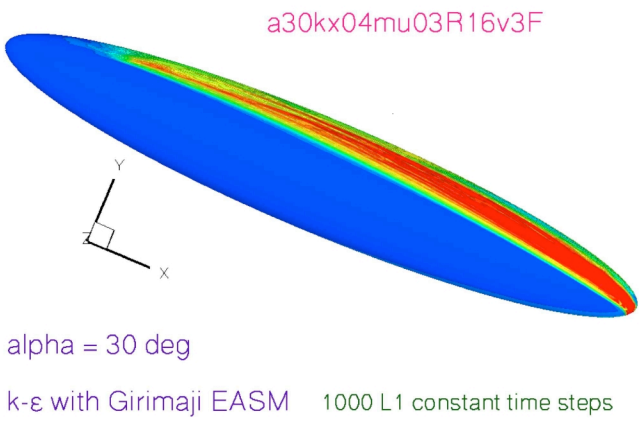

a. Distribution of $M_{t\text{-}max}$ plotted over the prolate spheroid surface

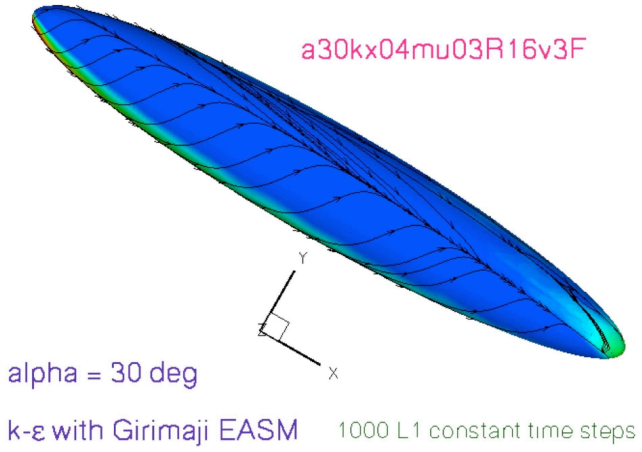

b. Computed surface streamline pattern

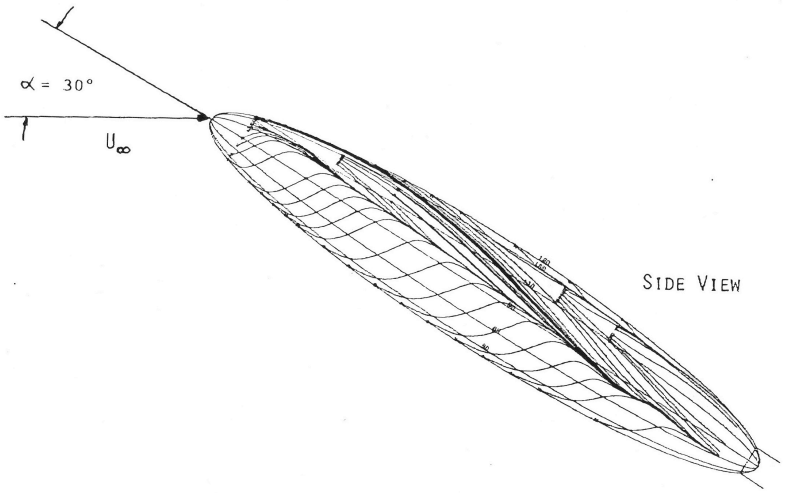

c. Surface streamlines integrated from measured velocity vector over the prolate spheroid (Kreplin, 1981).

Figure 10. Flow parameter contours and qualitative comparison to experiment solution at Re_L = 1.6E+6 and angle of attack at 30°, and $\mu_t/\mu_\ell\,|_{limit}$ = 0.30.

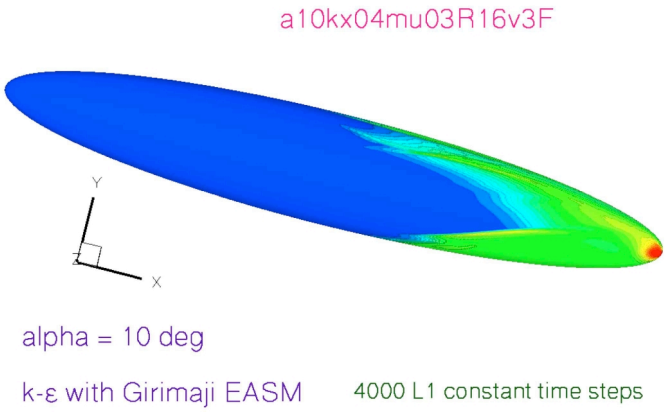

a. Distribution of $M_{t\text{-}max}$ plotted over the prolate spheroid surface

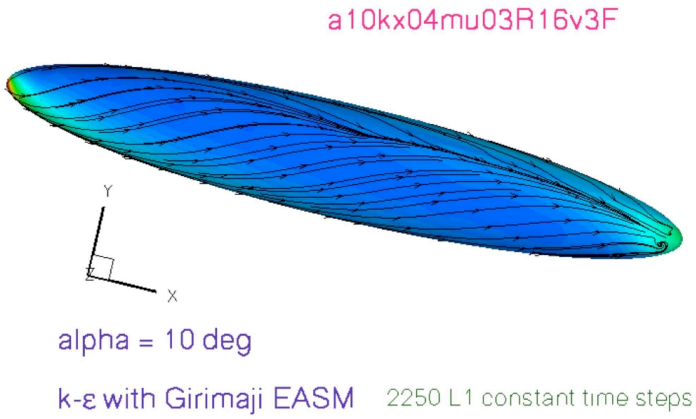

b. Computed surface streamline pattern

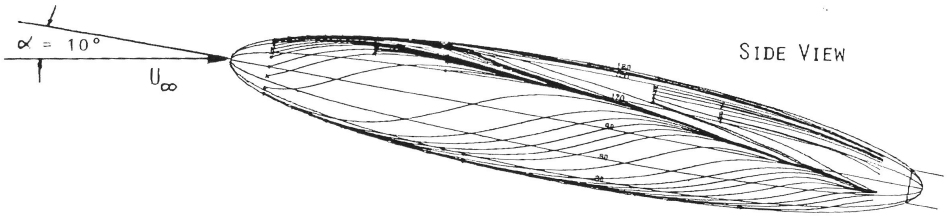

c. Surface streamlines integrated from measured velocity vector over the prolate spheroid (Kreplin, 1981).

Figure 11. Flow parameter contours and qualitative comparison to experiment solution at Re_L = 1.6E+6 and angle of attack at 10°, and $\mu_t/\mu_\ell\,|_{limit}$ = 0.30.